Editors' Suggestion

Nitrogen surface passivation of the Dirac semimetal Cd_3As_2

Luca Galletti,* Timo Schumann, Thomas E. Mates, and Susanne Stemmer
Materials Department, University of California, Santa Barbara, California 93106-5050, USA

(Received 24 September 2018; published 13 December 2018)

The influence of surface treatments on the transport properties of epitaxial films of the three-dimensional Dirac semimetal Cd_3As_2 is investigated. We show that exposure of the surface to a low-energy nitrogen plasma improves carrier mobilities, their temperature dependence, and allows for the observation of the quantum Hall effect in scaled thin films. The results provide insights into surface band bending as a function of the surface chemistry and the relative contributions of surface and bulk states to the measured transport properties.

DOI: 10.1103/PhysRevMaterials.2.124202

I. INTRODUCTION

The tetragonal II-V compound Cd_3As_2, long known for its high carrier mobilities [1], has recently been identified to belong to the family of three-dimensional Dirac semimetals [2–6]. In addition to bulk Dirac nodes (band crossings) such materials can also possess topologically nontrivial surface states [2,7,8]. Thin, quantum confined films of Cd_3As_2 grown by molecular beam epitaxy (MBE) exhibit the quantum Hall effect, which emerges at film thicknesses of around 60 nm and becomes virtually free of parallel, three-dimensional transport around 30-nm film thickness [9]. Although likely associated with surface states, the precise origin of the two-dimensional states that give rise to the quantum Hall effect is still being debated [9–12]. Recently, electric field gating experiments combined with Landau level spectroscopy and quantum capacitance measurements have shown that the carriers residing in the two-dimensional states are Dirac fermions [13]. These experiments used top gates with Al_2O_3 gate dielectrics deposited by atomic layer deposition. It was found that the two-dimensional carrier density increased by about a factor of 3 after deposition of the gate dielectric. This indicates that surface (interface) band bending effects and the defect chemistry of the Cd_3As_2 surface are important in this system.

Here, we show that the transport properties of Cd_3As_2 thin films depend strongly on the nature of the surface. In particular, adsorbed moisture leads to a significant contribution from *p*-type carriers with low carrier mobilities. We demonstrate that exposure to a low-energy N^* plasma leads to predominantly *n*-type conduction and significantly increases the measured Hall carrier mobilities for a wide range of film thickness. We discuss the importance of near-surface states in determining the transport properties and the role of surface band bending.

II. EXPERIMENTAL

Cd_3As_2 films were grown by MBE on ~120-nm-thick, epitaxial (111) GaSb buffer layers on (111) B-oriented GaAs substrates with a miscut of 1° toward $\langle\bar{1}\bar{1}2\rangle$. This results

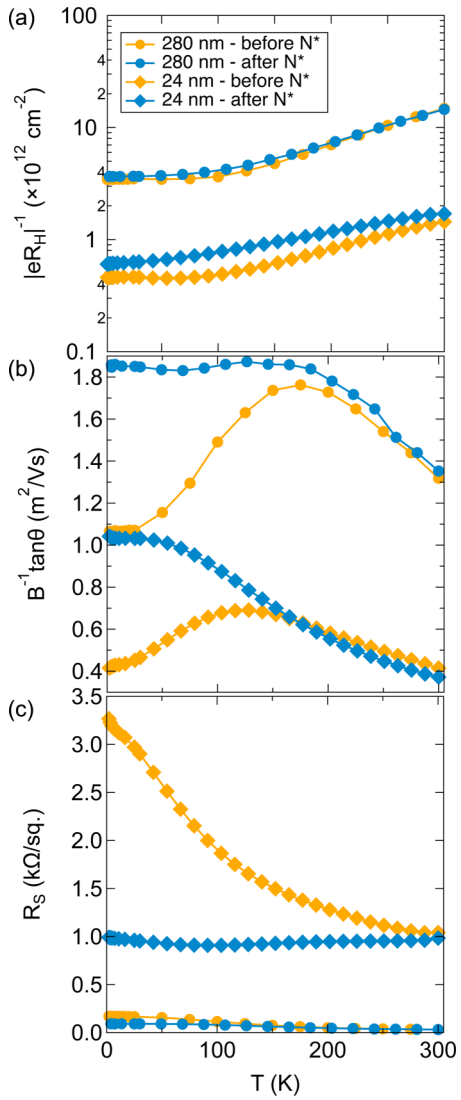

FIG. 1. Transport properties of Cd_3As_2 thin films with two different film thicknesses, 24 and 280 nm, before and after N^* surface treatment, respectively. (a) Inverse of the magnitude of the low-field Hall coefficient, $|(eR_H)^{-1}|$; (b) the carrier mobility, estimated from the low-field Hall effect and the sheet resistance, which is shown in (c). Measurements were carried out on a Hall bar structure.

*Corresponding author: luca_galletti@ucsb.edu

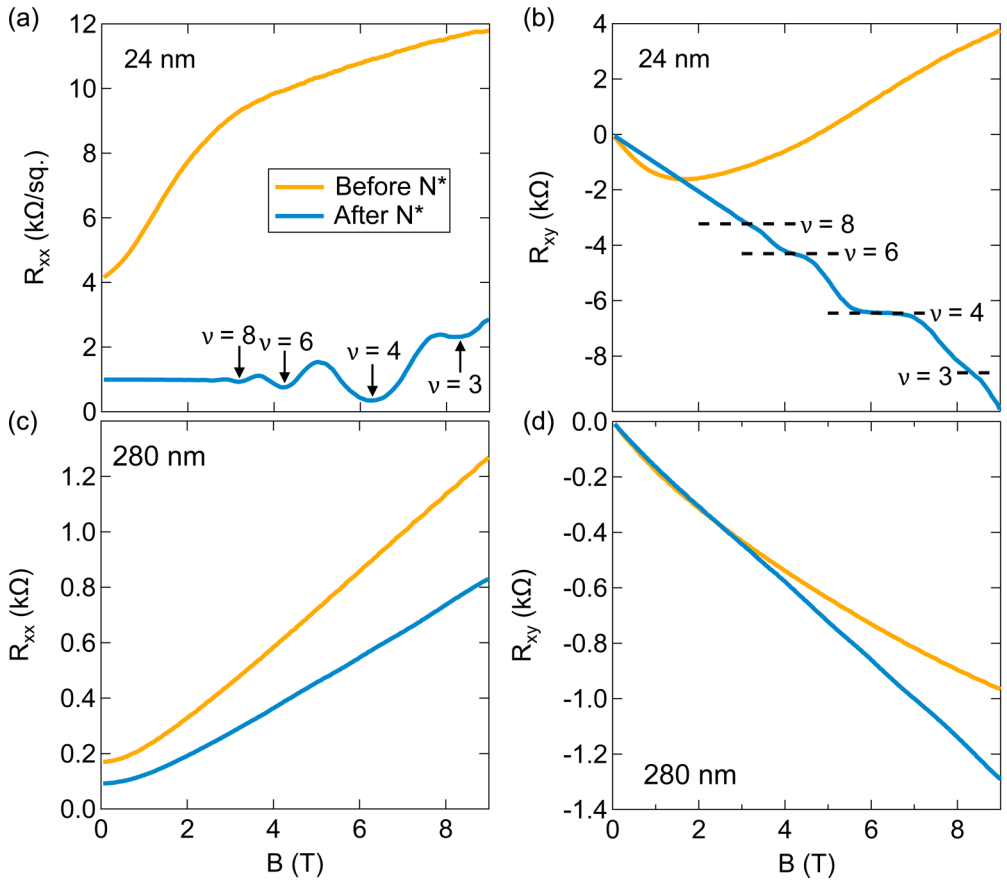

FIG. 2. Longitudinal and transverse magnetoresistances measured using a Hall bar structure before and after N* surface treatment of the Cd_3As_2 film surfaces. The data shown in panels (a) and (b) is from a 24-nm film, while that in panels (c) and (d) is from a 280-nm-thick film. To reduce the effects from intermixing between R_{xx} and R_{xy} the curves have been symmetrized (R_{xx}) and antisymmetrized (R_{xy}), respectively.

in epitaxial Cd_3As_2 films with their (112) surface planes parallel to the (111) planes of the cubic substrate/buffer [14]. Details about the MBE method and structural characterization of the films are described elsewhere [14,15]. Cd_3As_2 films of different thicknesses, ranging from 20 to 300 nm, were investigated. For measurements in van der Pauw configuration, Ti/Pt/Au top contacts were deposited by electron beam evaporation through a shadow mask. Magnetotransport measurements also used Hall bar structures, which were etched using standard lithography processes and Ar^+ dry etching. During dicing and processing, the sample surface was in contact with photoresist (AZ4210, NR1000Py and AZ5214). Measurements were performed in a Quantum Design Physical Properties Measurement System (PPMS). Longitudinal (R_{xx}) and transverse (R_{xy}) resistances were measured to determine the value of the sheet resistance (R_S). The value of the Hall coefficient ($R_H = R_{xy}/B$), where B is the magnetic field, was determined using a linear fit between -0.5 T and 0.5 T. The surfaces of selected films were exposed for 60 sec to an radio-frequency-generated N* plasma in an Ion Beam Deposition System (Veeco NEXUS IBD). The beam current and voltage were set to 200 mA and 60 V, respectively. The suppression voltage was 630 V. To reduce ion damage, the sample was kept at a high angle of 40° with respect to the incident direction of the N* plasma beam (for more details, please see the Supplemental Material [16]). X-ray photoelectron spectroscopy (XPS) was performed using Al Kα radiation (Kratos Axis Ultra XPS system). The energy positions of the peaks were calibrated with respect to the C 1s peak (285.0 eV binding energy).

III. RESULTS AND DISCUSSION

Figure 1 shows the temperature-dependent transport properties from thick (280 nm) and thin (24 nm) Cd_3As_2 films, respectively, before and after N* cleaning. Assuming that at low B, $R_H(B)$ is dominated by only one type of carrier, the density is given as $n = -(eR_H)^{-1}$. The tangent of the Hall angle, $\frac{1}{B}\tan\theta = |R_H|/R_{xx}$ can be used to define a Hall mobility (μ), $\tan\theta = \mu B$. Here, carriers of different sign (n and p) are contributing to the transport in untreated films, as discussed below. All films show indications of carrier freezeout at high temperatures (>100 K), while the carrier density at low temperatures is nearly constant [Fig. 1(a)]. Before cleaning, however, the presence of p-type carriers could cause some errors in this estimate, as we discuss below. As discussed previously [12,15], the constant carrier density at low temperatures can be understood as a signature of carriers in ungapped bulk and/or surface Dirac states. Thermal activation is observed at higher temperatures. In thin films, the bulk Dirac nodes are gapped but surface states are expected to remain ungapped to much lower film thicknesses

(∼5 nm) [17]. In analogy with topological insulators [18], the constant carrier density in thin films reflects the carriers in the metallic surface states, as discussed previously [12,13].

N* cleaning strongly affects the transport properties of the films. One consequence is a reduction in the density of p-type carriers, as we will discuss in more detail below, using the B-field dependence of R_{xy}. For the untreated films, the mobility exhibits nonmonotonic behavior as a function of temperature [Fig. 1(b)], with a maximum around 175 K, almost concurrent with the freezeout of a large fraction of the carriers. This mobility maximum is probably not an intrinsic property, but rather related to presence of multiple types of carriers of different sign. As a result, the number of n-type carriers are overestimated in a single carrier fit. Qualitatively similar behavior is also observed for thin films, despite the lower mobilities. The lower mobilities in the thin films can be understood as being due to a larger contribution of the transport in surface states [9,12], which suffer more from surface/interface scattering than bulk carriers. As shown in Fig. 1(c), after N* surface cleaning, the mobility shows a monotonic increase with decreasing temperature over the entire temperature range. The increase in mobility with N* surface cleaning is reflected in the lower sheet resistance [Fig. 1(c)], especially at low temperatures.

The longitudinal (R_{xx}) and transverse (R_{xy}) resistances as a function of magnetic field (B) for the 24-nm-thick film are shown in Figs. 2(a) and 2(b). As discussed previously, two-dimensional states dominate the transport characteristics in films of this thickness [9,12]. Before N* surface cleaning, the film shows a strong positive longitudinal magnetoresistance [Fig. 2(a)] and nonlinear Hall resistance [Fig. 2(b)]. A nonlinear $R_{xy}(B)$, and in particular the sign change at high B, indicates the presence of two types of carriers with different signs (n and p) and mobilities [19]. The observed behavior of $R_{xy}(B)$ indicates that the p-type carriers have lower mobilities and higher density that the n-type carriers. Native defects in Cd_3As_2 are believed to primarily affect scattering of hole carriers [6]. A more quantitative analysis, assuming two types of carriers, proved, however, not reliable as discussed in the Supplemental Material [16].

After the N* surface process, the film exhibits clear quantum Hall plateaus [Fig. 2(b)], at values of the transverse resistance $R_{xy} = \nu e^2/h$, where h is the Plank's constant and ν is the filling factor. In keeping with our earlier findings [9], the sequence of quantum Hall plateaus indicates a twofold degeneracy that is lifted at about 7 T, where $\nu = 3$ can be observed. The longitudinal resistance shows Shubnikov–de Haas oscillations on top of a constant background. The low-mobility p-type carriers are thus absent after the N* plasma treatment.

Thicker films do not show the quantum Hall effect. This is likely due to the fact that for these films, bulk-like states are dominating the transport. Before the N* surface cleaning, the 280-nm-thick film shows an almost linear longitudinal magnetoresistance [Fig. 2(c)] and a nonlinear Hall resistance [Fig. 2(d)]. The linear magnetoresistance has been attributed to be due to (microscopic) nonuniformities, such as n- and p-type puddles or defects [15,20,21]. The nonlinearity of the Hall resistance is less pronounced compared to that of the thin sample. After the surface process, the film shows a decrease in the longitudinal magnetoresistance and a linear Hall resistance up to 9 T, suggesting that also for thick samples, the low-mobility p-type carriers are absent after the N* surface process. The results show that nonmonotonic temperature dependence of the mobility of films without the N* plasma treatment [Fig. 1(b)] is likely a reflection of the presence of multiple types of carriers with different temperature dependencies of their densities and mobilities.

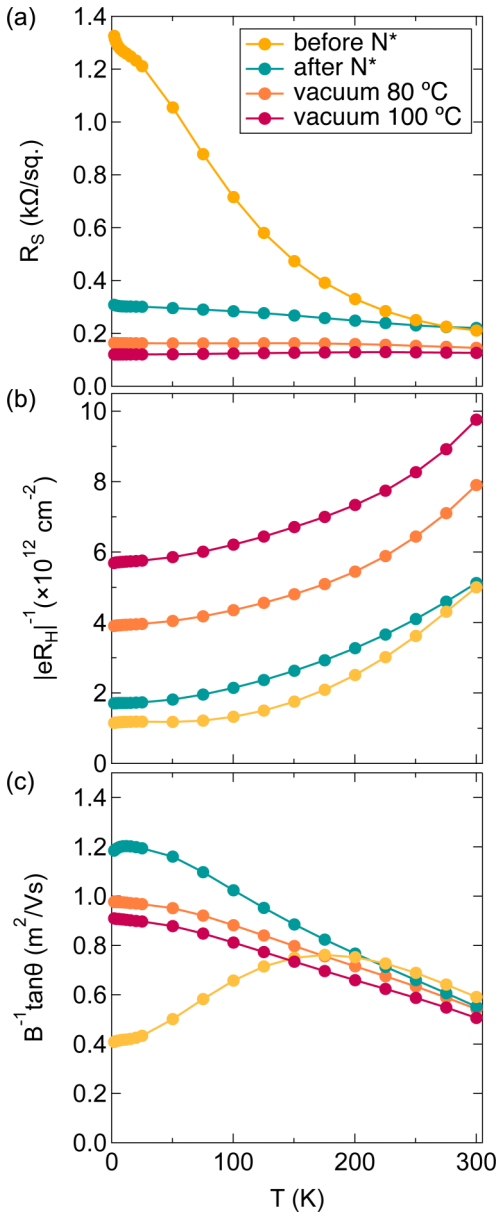

FIG. 3. Comparison of the transport properties of Cd_3As_2 thin films (50-nm thickness) before and after thermal annealing in the PPMS vacuum chamber and N* surface treatment, respectively. The sheet resistance is shown in (a), the inverse of the magnitude of the low-field Hall coefficient, $|(eR_H)^{-1}|$ in (b) and the extracted mobility in (c). The samples were measured in van der Pauw geometry. For same sample was measured, then annealed at 80 °C for 10 min, remeasured, then annealed to 100 °C for 10 min and remeasured. The N* treated film is from a different piece of the same sample.

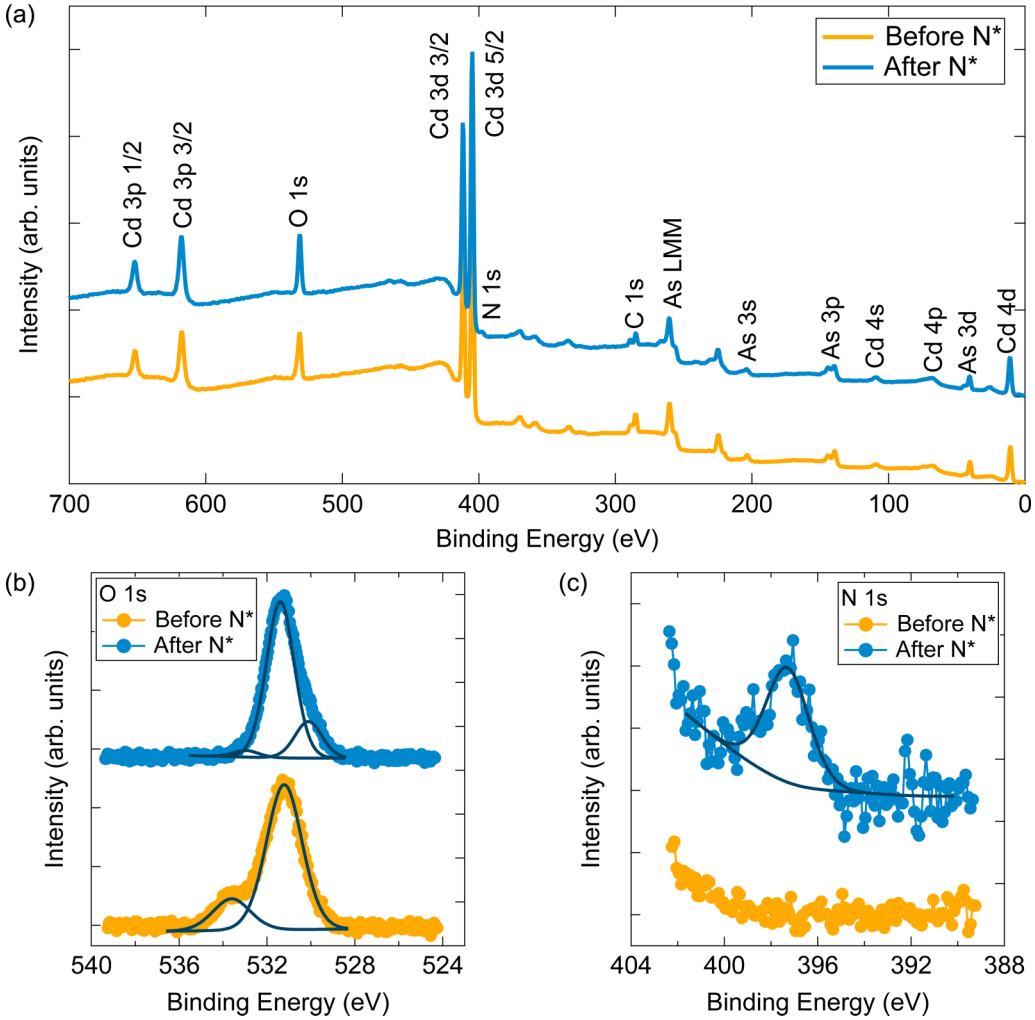

FIG. 4. XPS of the same Cd_3As_2 thin film (50-nm thickness) with and without N^* surface treatment. Panel (a) shows a survey scan, while panels (b) and (c) show high resolution spectra around the O 1s peak (b) and the nitrogen 1s peak (c), respectively. The lines show the components of fits to the peaks.

Transport properties similar to the N^* surface treatment can also be obtained by low-temperature thermal annealing in vacuum, as shown in Fig. 3 and Fig. S4 (Supplemental Material [16]). Regardless of the surface treatment (N^* vs vacuum anneal) the mobility increases monotonously with decreasing temperature, but the N^* cleaned film shows higher mobility. The vacuum annealed samples possess higher carrier concentrations, which indicates the formation of unintentional donor states, most likely associated with As vacancies [22].

To investigate the relationship between the transport properties and the physical properties of the surfaces, XPS measurements were performed on an untreated and on a N^* exposed film, respectively. Survey scans are shown in Fig. 4(a). Both types of films show peaks due to Cd and As core levels and As Auger lines [23]. Moreover, both samples show additional peaks from C 1*s* and O 1*s* states, likely from surface contamination upon air exposure. In addition to these similarities, the spectra show two relevant differences, namely the absence of a shoulder on the O 1*s* peak [Fig. 4(b)] and an extra peak around 398 eV [Fig. 4(c)] for the N^* cleaned film. The shoulder on the O 1*s* peak occurs at a binding energy of 533.6 eV, which is associated with hydrogenated oxygen, i.e., adsorbed moisture [23]. Thus, one likely origin of the predominantly *n*-type conduction after cleaning is associated with the removal of adsorbed, strongly electronegative OH^- species, which deplete the surface of electron carriers. The extra peak around 398 eV is consistent with nitrogen bonded to a metal. This indicates that the nitrogen can passivate surface dangling bonds, which would otherwise bond to OH^- species. This finding is similar to that for III-arsenide semiconductors, where it has been shown that nitrogen plasma treatments reduce interface trap states and passivate surfaces that are otherwise prone to surface Fermi level pinning [24].

IV. CONCLUSIONS

In summary, we have shown that the main effect of a nitrogen plasma passivation treatment of Cd_3As_2 film surfaces is that it affects the Fermi level position of the surface electronic states (surface band bending). For untreated, air-exposed surfaces, the Fermi level is located below the (gapped) Dirac point, giving rise to the presence of both *p*- and *n*-type carriers. The depletion of electron carriers from the surface

is attributed to (primarily) the effects of electronegative OH^- surface adsorbates detected in XPS. After exposure to N^*, the Fermi level near the surface shifts such that there is a accumulation of negative charge carriers in the surface states, resulting in only *n*-type conduction in both bulk and surface states. The mobility increases with N^* exposure, most likely due the elimination of low-mobility *p*-type carriers although additional gains in mobility from reduced surface defect scattering may also contribute. The quantum Hall effect can be observed with N^* exposure, provided that the contribution of bulk states is eliminated by confinement in sufficiently thin films. The results demonstrate the great sensitivity of the transport properties of Cd_3As_2 to the properties of their surfaces. This is consistent with the important role of topological surface states in the transport [13], as expected for a three-dimensional Dirac semimetal.

ACKNOWLEDGMENTS

The authors gratefully acknowledge support through by a grant from the U.S. Army Research Office (Grant No. W911NF-16-1-0280) and the Vannevar Bush Faculty Fellowship program by the U.S. Department of Defense (Grant No. N00014-16-1-2814). The work made use of the MRL Shared Experimental Facilities, which are supported by the MRSEC Program of the US National Science Foundation under Award No. DMR 1720256.

L.G. and T.S. contributed equally to this work.

[1] A. J. Rosenberg and T. C. Harman, J. Appl. Phys. **30**, 1621 (1959).

[2] Z. J. Wang, H. M. Weng, Q. S. Wu, X. Dai, and Z. Fang, Phys. Rev. B **88**, 125427 (2013).

[3] S. Borisenko, Q. Gibson, D. Evtushinsky, V. Zabolotnyy, B. Büchner, and R. J. Cava, Phys. Rev. Lett. **113**, 027603 (2014).

[4] Z. K. Liu, J. Jiang, B. Zhou, Z. J. Wang, Y. Zhang, H. M. Weng, D. Prabhakaran, S.-K. Mo, H. Peng, P. Dudin, T. Kim, M. Hoesch, Z. Fang, X. Dai, Z. X. Shen, D. L. Feng, Z. Hussain, and Y. L. Chen, Nat. Mater. **13**, 677 (2014).

[5] M. Neupane, S. Y. Xu, R. Sankar, N. Alidoust, G. Bian, C. Liu, I. Belopolski, T. R. Chang, H. T. Jeng, H. Lin, A. Bansil, F. Chou, and M. Z. Hasan, Nat. Commun. **5**, 3786 (2014).

[6] S. Jeon, B. B. Zhou, A. Gyenis, B. E. Feldman, I. Kimchi, A. C. Potter, Q. D. Gibson, R. J. Cava, A. Vishwanath, and A. Yazdani, Nat. Mater. **13**, 851 (2014).

[7] B.-J. Yang, and N. Nagaosa, Nat. Commun. **5**, 4898 (2014).

[8] P. J. W. Moll, N. L. Nair, T. Helm, A. C. Potter, I. Kimchi, A. Vishwanath, and J. G. Analytis, Nature (London) **535**, 266 (2016).

[9] T. Schumann, L. Galletti, D. A. Kealhofer, H. Kim, M. Goyal, and S. Stemmer, Phys. Rev. Lett. **120**, 016801 (2018).

[10] C. Zhang, A. Narayan, S. Lu, J. Zhang, H. Zhang, Z. Ni, X. Yuan, Y. Liu, J.-H. Park, E. Zhang, W. Wang, S. Liu, L. Cheng, L. Pi, Z. Sheng, S. Sanvito, and F. Xiu, Nat. Commun. **8**, 1272 (2017).

[11] M. Uchida, Y. Nakazawa, S. Nishihaya, K. Akiba, M. Kriener, Y. Kozuka, A. Miyake, Y. Taguchi, M. Tokunaga, N. Nagaosa, Y. Tokura, and M. Kawasaki, Nat. Commun. **8**, 2274 (2017).

[12] M. Goyal, L. Galletti, S. Salmani-Rezaie, T. Schumann, D. A. Kealhofer, and S. Stemmer, APL Mater. **6**, 026105 (2018).

[13] L. Galletti, T. Schumann, O. F. Shoron, M. Goyal, D. A. Kealhofer, H. Kim, and S. Stemmer, Phys. Rev. B **97**, 115132 (2018).

[14] T. Schumann, M. Goyal, H. Kim, and S. Stemmer, APL Mater. **4**, 126110 (2016).

[15] T. Schumann, M. Goyal, D. A. Kealhofer, and S. Stemmer, Phys. Rev. B **95**, 241113 (2017).

[16] See Supplemental Material at http://link.aps.org/supplemental/10.1103/PhysRevMaterials.2.124202 for additional studies of the influence of the N^* plasma parameters, for magnetoresistance data for thermally annealed films, and for two carrier fits of the magnetoconductance data.

[17] A. Narayan, D. Di Sante, S. Picozzi, and S. Sanvito, Phys. Rev. Lett. **113**, 256403 (2014).

[18] F. F. Tafti, Q. D. Gibson, S. K. Kushwaha, N. Haldolaarachchige, and R. J. Cava, Nat. Phys. **12**, 272 (2016).

[19] D. C. Look, *Electrical Characterization of GaAs Materials and Devices* (Wiley, New York, 1989).

[20] A. Narayanan, M. D. Watson, S. F. Blake, N. Bruyant, L. Drigo, Y. L. Chen, D. Prabhakaran, B. Yan, C. Felser, T. Kong, P. C. Canfield, and A. I. Coldea, Phys. Rev. Lett. **114**, 117201 (2015).

[21] T. Khouri, U. Zeitler, C. Reichl, W. Wegscheider, N. E. Hussey, S. Wiedmann, and J. C. Maan, Phys. Rev. Lett. **117**, 256601 (2016).

[22] D. P. Spitzer, G. A. Castellion, and G. Haacke, J. Appl. Phys. **37**, 3795 (1966).

[23] J. F. Moulder, W. F. Stickle, P. E. Sobol, and K. D. Bomben, *Handbook of X-ray Photoelectron Spectroscopy* (Perkin-Elmer Corporation, Eden Prairie, 1992).

[24] V. Chobpattana, J. Son, J. J. M. Law, R. Engel-Herbert, C. Y. Huang, and S. Stemmer, Appl. Phys. Lett. **102**, 022907 (2013).